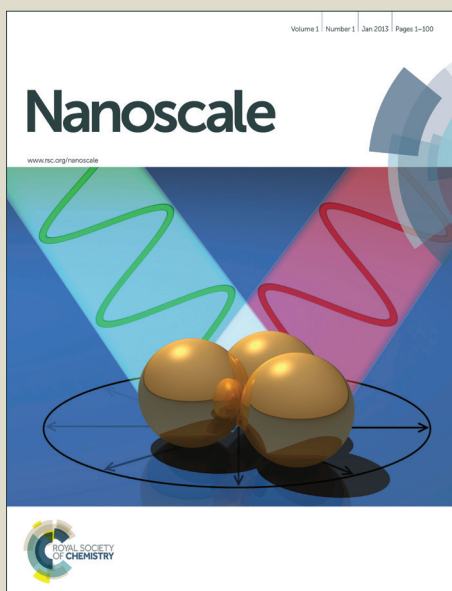


Nanoscale

Accepted Manuscript



This is an *Accepted Manuscript*, which has been through the Royal Society of Chemistry peer review process and has been accepted for publication.

Accepted Manuscripts are published online shortly after acceptance, before technical editing, formatting and proof reading. Using this free service, authors can make their results available to the community, in citable form, before we publish the edited article. We will replace this *Accepted Manuscript* with the edited and formatted *Advance Article* as soon as it is available.

You can find more information about *Accepted Manuscripts* in the [Information for Authors](#).

Please note that technical editing may introduce minor changes to the text and/or graphics, which may alter content. The journal's standard [Terms & Conditions](#) and the [Ethical guidelines](#) still apply. In no event shall the Royal Society of Chemistry be held responsible for any errors or omissions in this *Accepted Manuscript* or any consequences arising from the use of any information it contains.

ARTICLE

Templated Assembly of BiFeO₃ Nanocrystals into 3D Mesoporous Networks for Catalytic Applications†

Cite this: DOI: 10.1039/x0xx00000x

I. T. Papadas,^a S. S. Kota,^b M. G. Kanatzidis^{b,c} and G. S. Armatas^{*a}

Received 00th January 2012,

Accepted 00th January 2012

DOI: 10.1039/x0xx00000x

www.rsc.org/

Self-assembly of uniform nanocrystals into large porous architectures is currently of immense interest for nanochemistry and nanotechnology. These materials combine the respective advantages of discrete nanoparticles and mesoporous structure. In this article, we demonstrate a facile nanoparticle templating process to synthesize three-dimensional mesoporous BiFeO₃ material. This approach involves polymer-assisted aggregating assembly of 3-aminopropanoic acid-stabilized bismuth ferrite (BiFeO₃) nanocrystals followed by thermal decomposition of the surfactant. The resulting material consists of a network of tightly connected BiFeO₃ nanoparticles (~6–7 nm in diameter) and has a moderately high surface area (62 m² g⁻¹) and uniform pores (ca. 6.3 nm). As a result of the unique mesostructure, the mesoporous assemblies of BiFeO₃ nanoparticles show an excellent catalytic activity and chemical stability for the reduction of *p*-nitrophenol to *p*-aminophenol with NaBH₄.

Introduction

Bismuth ferrite (BiFeO₃) is a semiconductor that exhibits a strong coupled ferroelectric ($T_c \sim 1103$ K) and antiferromagnetic ($T_N \sim 657$ K) order at room temperature.¹ Thus, multiferroic BiFeO₃-based materials have been extensively investigated for applications such as high-performance lead-free ferroelectric and magnetoelectric devices, photovoltaic cells, new generation magnetic recording media, and spintronics.² Recently, considerable research efforts have been devoted to studying catalytic properties of BiFeO₃, especially, in the photocatalytic oxidation of water³ and the remediation of wastewater effluents such as oxidation of organic pollutants⁴ and degradation of dyes⁵. In this area, the BiFeO₃ has been proven to be promising catalyst mainly due to its narrow energy bandgap ($E_g \sim 2.2$ eV), high chemical stability⁶ and internal electric field originated by local ferroelectric polarization; such an electric field can induce separation of the photogenerated electron-hole pairs within the semiconducting structure^{2,7}. Moreover because of the weak ferromagnetism⁸, BiFeO₃ solid could be readily recycled from the reaction mixture by applying an external magnetic field.⁹ This prevents the loss of catalyst and renders the catalyst cost-effective.

It is well known that creating materials with regular porosity at the mesoscale is an effective approach to improve catalytic, magnetic and electronic properties. These materials not only combine the functional properties of the framework

constituents, such as chemical reactivity, photon-to-electron conversion ability and electron mobility, but also the advantages of a mesoporous structure such as large number of active sites and strong interfacial interactions between the material's surface and reactants.¹⁰ Although BiFeO₃ nanoparticles (NPs) with variable sizes and shapes have been prepared^{6,11}, synthesis of porous architectures from BiFeO₃ NPs with accessible pore volume is still challenging. So far synthetic efforts have resulted in mesoporous BiFeO₃ hollow spheres¹² and BiFeO₃ mesocrystals¹³ on using solid state transformation of Fe,Bi-glycerol chelates and Bi-containing Prussian blue (Bi[Fe(CN)₆] \cdot 4H₂O) polymers, respectively. These materials, however, cannot be obtained as crystalline products with retention of porosity, and therefore they manifested nanocrystalline property with limiting surface area. Furthermore, mesoporous silica with embedded BiFeO₃ nanocrystals¹⁴ and nanoporous BiFeO₃ nanocrystalline thin films¹⁵ have been prepared through soft templating approach. Indeed these BiFeO₃-based mesostructures exhibited good catalytic activity for the degradation of dyes under visible light. More recently, we described a hard-templating method to synthesizing mesoporous BiFeO₃ semiconductor. We utilized infiltration and inverse replica solidification of tartrate-chelated Bi(III) and Fe(III) metal precursors inside the pores of carbon template to produce well-ordered mesoporous BiFeO₃.¹⁶ The obtained material possesses a nanoscale pore structure with hexagonal symmetry, and it exhibited a high oxygen evolution reaction activity with long-term cycling stability.

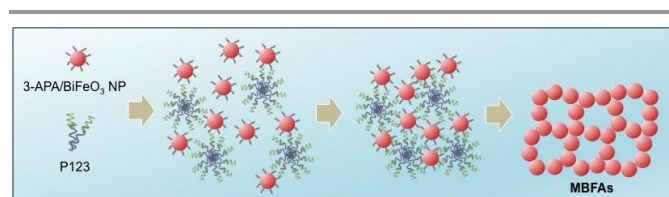
Here we present a facile nanoparticle templating process, which involves a surfactant-directed self-assembly of ligand-stabilized BiFeO₃ NPs, for the synthesis of unique mesoporous BiFeO₃ NP-based network. The framework structure of this material consists solely of interconnected BiFeO₃ NPs and exhibits internal porosity with large pore volume. Because of the three-dimensional (3D) open-pore structure, nearly all BiFeO₃ NPs are exposed to the reactants showing high catalytic activity and chemical stability in the reduction of *p*-nitrophenol into *p*-aminophenol under mild conditions. To the best of our knowledge, this is first report addressing functionality of BiFeO₃ material for the reduction of nitro-compounds with NaBH₄.

Results and discussion

Synthesis and structural properties

Mesoporous assemblies of BiFeO₃ NPs (denoted as MBFAs) were realized by first surface modification of individual BiFeO₃ nanocrystals with 3-aminopropanoic acid (3-APA) and then using a templated assembly of these nanoparticle colloids in the presence of surfactant aggregates. A schematic overview of the synthesis procedure is illustrated in Scheme 1. In particular, BiFeO₃ NPs with a diameter of about 6 nm were synthesized by high temperature liquid-phase synthesis using previously reported method.¹⁷ In our colloidal approach, soluble ligand-stabilized BiFeO₃ NPs are prepared by treatment with 3-APA in water. This colloidal solution constitutes the starting material from which mesoporous networks can be assembled by polymer templating. The specific advantage of using 3-APA as surface ligand is that its carboxyl (–CO₂H) group can coordinate to the nanoparticle surface, while the amine end group can prevent nanoparticle aggregation and stabilizes the colloidal solution. In addition, the –NH₂ function is expected to interact with the polar fragment of surfactant during the assembly process. Because of the small size, 3-APA could also enable direct NP–NP interactions upon ligand removal at the growth temperature, thus yielding tightly interconnected NP-based networks. To verify the coordination of 3-APA to the nanoparticle surface, the infrared (IR) spectrum of 3-APA-capped NPs was compared to that of 3-APA compound alone (Fig. S1†). The carbonyl (C=O) stretching vibrations of 3-APA are readily observed at ~1634 cm⁻¹ and 1392–1414 cm⁻¹ region¹⁸, while a remarkable bathochromic/red shift in its peak position (by ~10–15 cm⁻¹) emerged for hybrid NPs. No considerable changes in the frequencies of the C–N stretching (~846 cm⁻¹) and –NH₂ bending (~1574 cm⁻¹) bands are observed after surface treatment. This justifies that 3-APA molecules are strongly bonded to the nanoparticle surface through the carboxylic acid group. The weight fraction of 3-APA grafted on the surface of BiFeO₃ NPs was estimated to be ~7.2%, according to the thermogravimetric (TG) analysis measurements (Fig. S2†).

For a typical synthesis of MBFAs, amphiphilic poly(ethylene oxide)-*block*-poly(propylene oxide)-*block*-poly(ethylene oxide) (EO₂₀PO₇₀EO₂₀) copolymer was added to an aqueous dispersion of 3-APA-capped BiFeO₃ NPs under vigorous stirring. Then, during the slow evaporation of solvent, the soluble BiFeO₃ NPs will preferentially incorporate within the polar PEO chains of surfactant micelles, yielding mesostructured organic/BiFeO₃ composites. Key parameters that dictate pore morphology of the final product involve the weight fraction of inorganic materials in the reaction mixture and the rate of assembly process. This step was evaluated by varying the amount of colloidal BiFeO₃ NP solution and the solvent evaporation time, for instance, by evaporating the mixture in open vessels with different exposed surfaces. Overall, when the nanoparticles content is typically lower than 50% or higher than 90% by weight (relative to surfactant) or even the evaporation of solvent is considerably fast (*i.e.*, within a few hours), the assembly process resulted in the formation of bulky precipitates or nanoparticle aggregates with limited porosity. This was evidenced with N₂ physisorption measurements (results not shown). The optimal reaction mixture had a BiFeO₃:surfactant (w/w) ratio of 0.7:1 with a surfactant concentration of 7 wt %, and allowed to evaporate for 7–8 days. A 3D mesoporous network of BiFeO₃ NPs with accessible pore channels was obtained after fusing nanoparticles together and removing template by a calcination process. Details of the synthesis procedure are described in Experimental Section. The complete elimination of the polymer template was verified by TG analysis. The TG curve of the mesoporous sample shows no appreciable weight loss in the 50 – 480 °C range; then a mass loss of ~1.8% was observed up to 600 °C possibly due to the dehydroxylation of surface (Fig. S3†).



Scheme 1. Schematic illustration showing possible reaction route for the formation of mesoporous BiFeO₃ nanoparticle assemblies (MBFAs).

To characterize the structure of MBFAs, we used a combination of small-angle X-ray scattering (SAXS), X-ray diffraction (XRD) and transmission electron microscopy (TEM). Fig. 1a shows SAXS pattern of the template-free sample, in which a single broad scattering peak centered at q ($= 4\pi \cdot \sin\theta/\lambda$) range of 0.52 nm⁻¹ can be clearly observed, suggesting mesoscale order. The angular position of this peak is associated with an average center-to-center interparticle distance ($d=2\pi/q$) of about 12.1 nm. Analysis of the scattering data using the indirect transform program GNOM¹⁹ gave a quite narrow distribution of particle size with an average diameter of ~6.8 nm (Fig. 1a, inset). This value is very close to the average particle size of starting material found from TEM

(~ 6.2 nm, Fig. S4[†]), consistent with the fact that the particle size, established through colloidal synthesis, does not change during assembly and annealing process.

The wide-angle XRD analysis confirms that the perovskite BiFeO_3 structure is the only crystal phase in mesoporous sample; all the diffraction peaks correlate well to the reference data for BiFeO_3 with rhombohedral $R3c$ lattice ($a_{\text{hex}} = b_{\text{hex}} = 5.58$ Å and $c_{\text{hex}} = 13.87$ Å, JCPDS card no. 86-1518), see Fig. 1b. The average crystal size of BiFeO_3 , calculated using the Scherrer equation and the width of the (110) peak, was estimated to be ~ 12 nm, which is fairly larger than the diameter of the component nanoparticles. Such a variation indicates that the thermal process has resulted in a growth of the grain size of precursor BiFeO_3 NPs. This is also consistent with the TEM images that show tightly connected nanoparticles comprising the pore walls of the MBFAs material (see below).

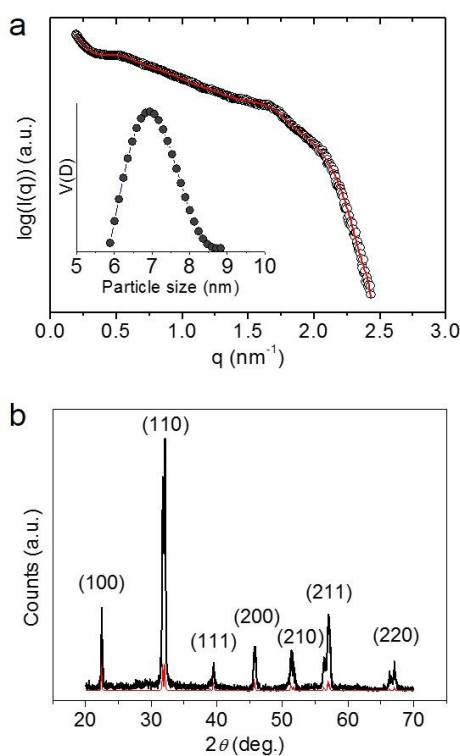


Fig. 1 (a) Small-angle X-ray scattering (Inset: particle size distribution of constituent BiFeO_3 NPs derived from scattering data) and (b) X-ray diffraction pattern for mesoporous BiFeO_3 NP assemblies (MBFAs). The red line in panel (b) shows the calculated XRD curve of rhombohedral BiFeO_3 (JCPDS card no. 86-1518). In panel (a): the red line is fit to the data.

Fig. 2 display typical TEM images and the selected area electron diffraction (SAED) pattern obtained from MBFAs. It can be seen clearly that this material is constructed of small NPs as building blocks, the diameter of which is ~ 6 nm, connecting together and form 3D mesoporous structure. This is in agreement with the analytic results from SAXS. A high magnification image also confirms that uniform mesopores with a diameter of ~ 6 – 7 nm are arranged in a disordered fashion within the assembled network (Fig. 2b). The crystal structure of the MBFAs was further examined with high-

resolution TEM (HRTEM) and electron diffraction measurements. HRTEM image reveals that the constituent BiFeO_3 NPs possess single-phase perovskite structure with high crystallinity. In Fig. 2c the regular spacings of the lattice fringes are about 2.8 Å, which matched reasonably well with the distances between the (210) and (110) crystal planes (along the [001] zone axis, as evident from Fast Fourier Transform (FFT) analysis, inset of Fig. 2c) of rhombohedral BiFeO_3 . The SAED pattern taken from a small area of the mesoporous structure indicated a multicrystalline character, showing a series of Debye-Scherrer diffraction rings (Fig. 2d). All the electron diffraction rings can be readily assigned to the rhombohedral symmetry of BiFeO_3 . Moreover, examination of the chemical composition of MBFAs by energy-dispersive X-ray spectroscopy (EDS) showed a Bi:Fe molar ratio of $\sim 1:1$, which is consistent with the stoichiometry of BiFeO_3 (Fig. S5[†]).

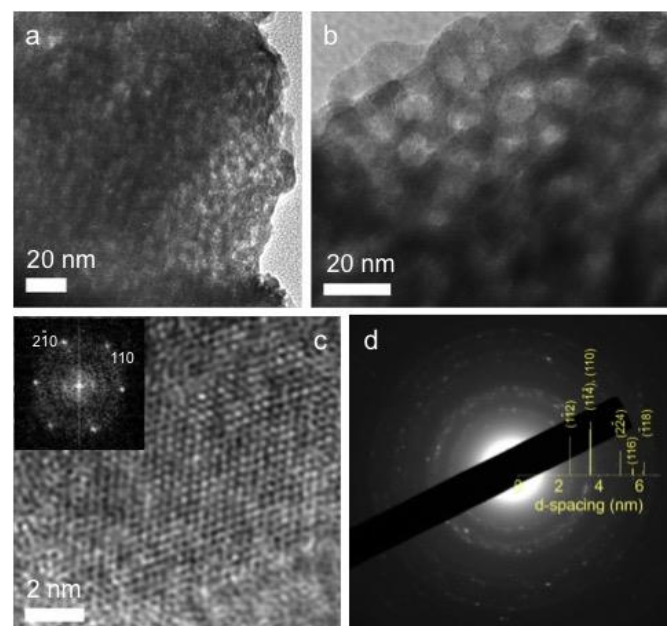


Fig. 2 (a and b) Typical TEM images, (c) high-resolution TEM obtained from an individual nanoparticle (Inset: the corresponding fast-Fourier transform (FFT) pattern) and (d) selected-area electron diffraction (SAED) of mesoporous BiFeO_3 NP assemblies (MBFAs). The FFT pattern in panel (c) can be indexed to the [001] zone of rhombohedral BiFeO_3 phase (space group: $R3c$).

Nitrogen physisorption measurements indicate that MBFAs has an accessible pore structure and contains uniform mesopores between the nanoparticles (Fig. 3a). It exhibits a type IV adsorption curve with a H_3 -type hysteresis loop according to IUPAC classification, which is characteristic of mesoporous solids with 3D interconnected porosity.²⁰ The Brunauer-Emmet-Teller (BET)²¹ surface area and pore volume of the MBFAs were measured to be 62 m^2 g^{-1} and 0.11 cm^3 g^{-1} , respectively. In comparison, we obtained a surface area of ~ 8 m^2 g^{-1} and pore volume of ~ 0.01 cm^3 g^{-1} for non-templated counterpart (Fig. S6[†]) that was formed by randomly aggregated BiFeO_3 NPs. These results clearly suggest that the proposed method is a typical template-driven synthesis process. The pore size distribution plot derived from the adsorption data using the

density function theory (NLDFT)²² (based on slit-like pores) shows a porous structure with uniform mesopores of ~ 6.3 nm (Fig. 3a, inset), consistent with TEM results. Given an average nanoparticle diameter of 6.8 nm (determined by SAXS analysis), the sum of the pore diameter and the nanoparticle size is approximately commensurate with the average repeat distance obtained from SAXS (ca. 12.1 nm). This indicates that the wall thickness of the MBFAs is about one nanoparticle thick.

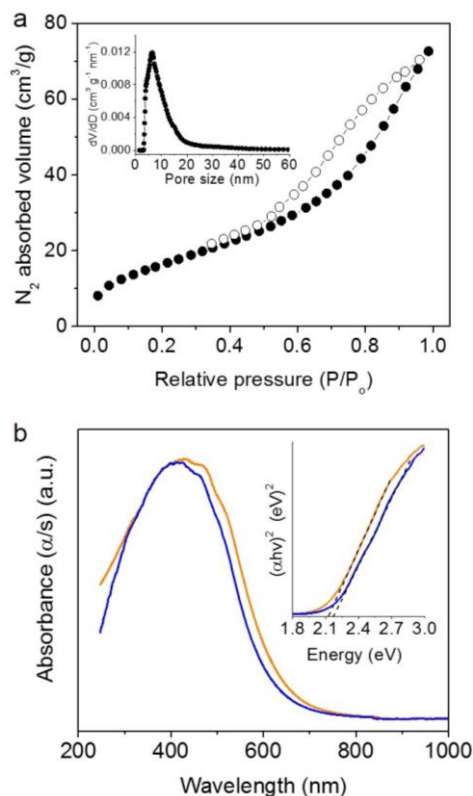


Fig. 3 (a) Nitrogen adsorption-desorption isotherms at 77 K and the corresponding NLDFT pore size distribution (inset) and (b) UV-vis/NIR diffuse reflectance spectra for mesoporous BiFeO₃ NP assemblies (MBFAs) (blue line) and randomly aggregated BiFeO₃ NPs (orange line). The inset in panel (b) shows the corresponding $(\alpha hv)^2$ versus hv plots.

Fig. 3b shows the diffuse reflectance UV-visible/Near-IR (UV-vis/NIR) spectrum of the mesoporous assemblies from BiFeO₃ NPs (MBFAs) as well as that of non-templated BiFeO₃ analogue. The MBFAs shows an intense optical absorption onset in the visible region (570 nm), which is associated with an energy gap transition at 2.17 eV according to the $(\alpha hv)^2$ vs energy plot (see Fig. 3b, inset).²³ Relative to the non-templated BiFeO₃ (2.12 eV), MBFAs shows a distinct (0.5 eV) blue shift in the band gap. This small observed shift may be associated with the nanometric structure and different grain composition of MBFAs.²⁴

Catalytic study

Owing to the large porosity and internal surface area, MBFAs hold promise for applications in catalysis. The catalytic

properties of the MBFAs material were examined in reduction of *p*-nitrophenol (4-NP) into *p*-aminophenol (4-AP) using NaBH₄ as reducing agent. In general, 4-AP is an important intermediate in manufacturing analgesic drugs, drying agents, and anticorrosion lubricants.²⁵ All the catalytic reactions were performed in a quartz reactor and the product evolution was monitored by UV-visible spectroscopy. It was found that MBFAs, even with a relative low concentration of reducing agent ($C_{\text{NaBH}_4}/C_{4\text{-NP}} = 50$), quantitatively convert 4-NP in 4 min (Fig. 4a). As the reaction proceeds, the characteristic absorption peak of *p*-nitrophenolate ions at 400 nm²⁶ decreases rapidly and completely disappears after 4 min. Meanwhile, a new absorption band appears at ~ 300 nm, addressing the formation of 4-AP (Fig. S7†). Comparatively, when the same amount of randomly aggregated BiFeO₃ NPs was introduced into the solution, the reduction reaction proceeded almost quantitatively (98%, in 5 min), but at a less efficient rate. Control experiments conducted in the absence of either catalyst or NaBH₄ did not indicate appreciable transformation of 4-NP under the present conditions (see Fig. 4a, inset), suggesting that reduction of 4-NP is a catalytic process.

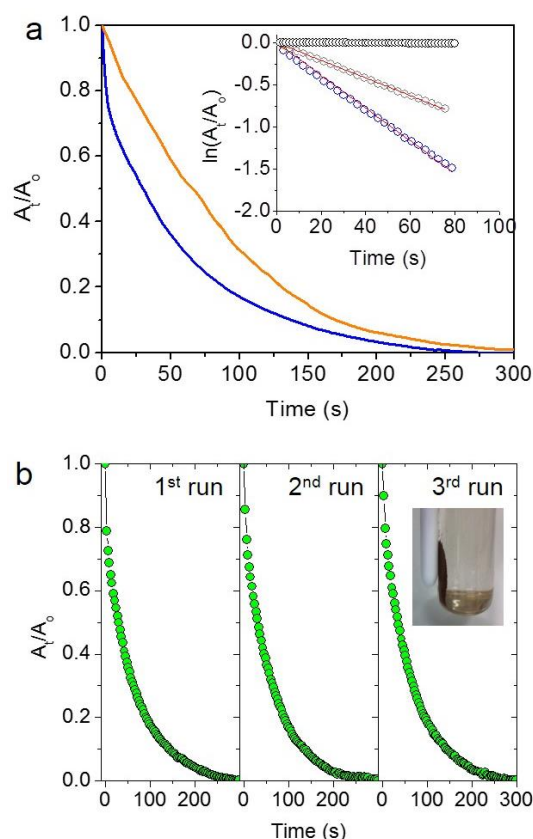


Fig. 4 (a) Time dependent reduction of *p*-nitrophenol (4-NP) to *p*-aminophenol (4-AP) catalyzed by mesoporous BiFeO₃ NP assemblies (MBFAs) (blue line) and randomly aggregated BiFeO₃ NPs (orange line) (where, A_0 and A_t are the initial and final (at time t) absorbance of 4-NP at $\lambda = 400$ nm, respectively). Inset: The corresponding kinetic plots of $\ln(A_t/A_0)$ versus time. The corresponding red lines are fit to the data. The kinetic analysis plot of 4-NP reduction with NaBH₄ in the absence of catalyst is also given (black symbols). (b) Catalytically recyclable reduction of 4-NP by MBFAs. Inset: Isolation of MBFAs catalyst using an external magnetic field.

The reaction follows a pseudo-first-order rate law as indicated from the linear plots of $\ln(A_t/A_0)$ vs time (Fig. 4a, inset) and, therefore, the apparent reaction rate constant (k_{app}) can be obtained as a slope of the linear fits. The results showed that the MBFAs ($k_{app} = 0.018 \text{ s}^{-1}$) achieves 2 times faster reduction rate than that from random BiFeO_3 NP aggregates (0.009 s^{-1}). This comparison demonstrates that the superior activity of the MBFAs is associated with the 3D open-pore structure and large pore volume, which provide high density of active sites and efficient diffusion of reactants and reaction products between the nanoparticles. Notable, the catalytic activity of MBFAs compared higher or even comparable to that of other high-performance catalysts (see Table S1†). For example, MBFAs outperforms dumbbell-like $\text{Au/Fe}_3\text{O}_4$ NPs²⁷, Au/CuO microparticles²⁸, Cu/Ag NPs²⁹, Pd/polypyrrole nanocapsules³⁰ and dendritic Ag/Au nanostructures³¹, while it nearly as effective as the Pd/Ag bimetallic dendrite³² and $\text{Fe}_3\text{O}_4/\text{graphene/M}$ ($M=\text{Pt, Pd, PtPd}$) composite³³ catalysts studied under similar reaction conditions.

It is noteworthy that the assembled structure of MBFAs appears to be held by strong interparticle bonds and it remains stable during catalysis. At the end of the catalytic reactions, the MBFAs can be recovered easily from the reaction mixture using an external magnet and can be reused for the next catalytic run. As shown in Fig. 4b, the recovered catalyst can be successfully recycled and reused for at least three successive runs with stable catalytic efficiency ($k_{app}^1 = k_{app}^2 = k_{app}^3 = 0.018 \pm 0.001 \text{ s}^{-1}$). According to the textural data provided by N_2 adsorption, the reused catalyst maintains the surface area and pore volume of the fresh sample, thus indicating high stability and reusability in the present conditions.

Conclusions

In conclusion, 3D mesoporous network of interconnected BiFeO_3 NPs has been prepared through a facile nanoparticle templating process. The synthesis is accomplished by a polymer-templated aggregating assembly of uniform BiFeO_3 NPs (6–7 nm in diameter) stabilized with 3-aminopropanoic acid (3-APA) ligands. Mesoporous assemblies of BiFeO_3 NPs, which exhibit large accessible pore surface ($62 \text{ m}^2\text{g}^{-1}$) and uniform pores (ca. 6.3 nm), showed to be highly effective in the reduction of *p*-nitrophenol to *p*-aminophenol with NaBH_4 . Indeed, the enhancement of catalytic properties (compared to the non-templated analogue) is considered to be due to the large porosity and high density of active sites. The present chemical route for templating 3-APA-capped nanoparticles into 3D porous networks represents a viable method for the deliberate construction of new functional porous materials with intrigued characteristics, including catalytic activity and magnetic susceptibility.

Experimental

Preparation of colloidal BiFeO_3 NPs

BiFeO_3 NPs were prepared according to a modified literature procedure.³⁴ Briefly, equimolar amounts (0.2 mmol) of $\text{Bi}(\text{NO}_3)_3$, $\text{Fe}(\text{NO}_3)_3$ and tartaric acid dissolved in 20 mL of 2 N HNO_3 were heated at 150 °C under continuous stirring until complete evaporation of the solvent. The dry green powder was then decomposed in air at 300 °C for 2 h. In a typical surface modification reaction, as-made BiFeO_3 NPs were added in deionized (DI) water containing 3-aminopropanoic acid (3-APA), and the pH was adjusted to 4.0 with 1 N HNO_3 . The resulting mixture was then vigorously stirred at room temperature to assure that nanoparticles will transfer to the liquid phase and form stable suspension, typically within 24 h. Dispersion was initially assisted with sonication for about 20 min. The amount of 3-APA used was determined relative to the mole amount of precursor BiFeO_3 NPs; the targeted BiFeO_3 :3-APA ratio was ~1:0.9. The 3-APA-capped BiFeO_3 NPs were isolated by centrifugation, washed with water twice, and dried under vacuum at 80 °C for 12 h. A stable colloidal solution (63 mg mL^{-1}) solution was obtained by dispersing the 3-APA-capped BiFeO_3 NPs in DI water.

Synthesis of MBFAs

Mesoporous BiFeO_3 nanoparticle assemblies (MBFAs) were prepared as follows: 0.14 g of $\text{EO}_{20}\text{PO}_{70}\text{EO}_{20}$ triblock copolymer was added to a colloidal solution of BiFeO_3 NPs (2 mL) with continuous stirring for 2 h at room temperature. Subsequently, the solution contents were transferred to an oven at 40 °C and left undisturbed until a yellow-brown colored gel was formed, typically within 7 days. Removal of surfactant was achieved by annealing the gel product at 360 °C for 6 h in air, using a 0.5 °C min^{-1} heating rate. For comparative studies random aggregates of BiFeO_3 NPs were prepared according to the above procedure, but in the absence of template. To purify the MBFAs, the as-synthesized material was suspended in chloroform (10 mg mL^{-1}) by ultrasonication for 10 min. The less dense MBFAs phase forms a stable suspension whereas the by-products, *i.e.* dense BiFeO_3 particles, sink. The suspension was decanted carefully with a pipette and the MBFAs product was isolated by centrifugation, washed with DI water and ethanol, and dried at 80 °C under vacuum for 12 h.

Physical characterization

Thermogravimetric (TG) measurements were performed on a Perkin-Elmer Diamond system. Thermal analysis was conducted from 40 to 600 °C in air atmosphere (100 mL min^{-1} flow rate) with a heating rate of 5 °C min^{-1} . Infrared (IR) spectra were recorded on a Perkin Elmer Model Frontier FT-IR spectrometer with 2 cm^{-1} resolution. Samples were prepared as KBr pellets. Small-angle X-ray scattering (SAXS) measurements were performed on a Rigaku S-MAX 300 high-brilliance system using $\text{Cu K}\alpha$ radiation (80 kV and 40 mA). Measurements were performed by transmission in samples that gently grounded and held in a quartz capillary tube (inner diameter of 1 mm). The sample-to-detector distance and center of the beam were precisely measured using a Ag-behenate standard ($d_{001} = 58.38 \text{ \AA}$). The two-dimensional diffraction

images were integrated into a one-dimensional diffraction pattern, as a function of q , with the Fit2D program³⁵. Scattering data were corrected for dark current and empty tube scattering. Wide-angle X-ray diffraction (XRD) patterns were recorded on a PANalytical X'pert Pro MPD powder diffractometer with a Cu $K\alpha$ rotating anode source ($\lambda=1.5418 \text{ \AA}$) and operated at a generator voltage and an emission current of 40 kV and 45 mA, respectively. Nitrogen adsorption-desorption isotherms were measured at 77 K on a Quantachrome Nova 3200e sorption analyzer. Before analysis, all samples were degassed at 150 °C under vacuum ($<10^{-5}$ Torr) for 12 h. The specific surface areas were calculated by applying the Brumauer-Emmett-Teller (BET) method to the adsorption isotherms in the 0.05 – 0.25 relative pressure (P/P_0) range. Samples were degassed at 150 °C for about 12 h prior to the analysis. The total pore volumes were derived from the adsorbed volume at $P/P_0 = 0.95$. Transmission electron microscope (TEM) images and electron diffraction patterns were recorded on a JEOL JEM-2100 microscope operating at an accelerating voltage of 200 kV. The samples were prepared by placing a drop of a dilute ethanol dispersion of fine powders on a carbon-coated Cu grid. Quantitative microprobe analyses were performed on a JEOL JSM-6390LV scanning electron microscope (SEM) equipped with an Oxford INCA PentaFET-x3 energy dispersive X-ray spectroscopy (EDS) detector. Data acquisition was performed with an accelerating voltage of 20 kV and 60 s accumulation time. Diffuse reflectance UV–vis/NIR spectra were recorded at room temperature with a Perkin Elmer Lambda 950 optical spectrophotometer equipped with an integration sphere, using powder BaSO₄ as a 100% reflectance standard. The Kubelka-Munk equation $\alpha/S = (1-R)^2/(2R)$ (where R is the measured reflectance and α , S are the absorption and scattering coefficients, respectively), was used to convert the reflectance data to absorbance.

Catalytic reactions

The catalytic reactions were carried out in a quartz cuvette with 1-cm path length containing BiFeO₃ catalyst (1 mg mL⁻¹), *p*-nitrophenol (4-NP) (0.1 mM) and NaBH₄ (5 mM). The product evolution was monitored by UV–vis spectroscopy using a Perkin Elmer Lambda 25 spectrophotometer. For recycling experiments, the catalyst was isolated by centrifugation or using a magnet, washed with DI water and ethanol several times, dried at 200 °C for 2 h, and used for the next catalytic run.

Acknowledgements

We acknowledge support from the Greek Ministry of Education (NSRF) and the European Union under the ERC Grant Schemes (ERC-09, MESOPOROUS-NPs) and THALES project (MIS 80802).

Notes and references

- ^a Department of Materials Science and Technology, University of Crete, Heraklion 71003, Crete, Greece, E-mail: garmatas@materials.uoc.gr
- ^b Department of Chemistry, Northwestern University, Evanston, IL 60208, USA
- ^c Materials Science Division, Argonne National Laboratory, Argonne, IL 60439, USA
- † Electronic Supplementary Information (ESI) available: IR spectra and TG profiles of as-made BiFeO₃ NPs and MBFAs sample, TEM images of 3-APA-capped BiFeO₃ NPs, EDS spectrum of MBFAs, N₂ adsorption–desorption isotherms of randomly aggregated BiFeO₃ NPs and catalytic data for 4-NP reduction by MBFAs and other nanostructured catalysts. See DOI: 10.1039/b000000x/
- G. Catalan and J. F. Scott, *Adv. Mater.*, 2009, **21**, 2463.
 - T. Choi, S. Lee, Y. J. Choi, V. Kiryukhin and S.-W. Cheong, *Science*, 2009, **324**, 63; N. Hur, S. Park, P. A. Sharma, J. S. Ahn and S. Guha, *Nature*, 2004, **429**, 392; J. Wang, J. B. Neaton, H. Zheng, V. Nagarajan, S. B. Ogale, B. Liu, D. Viehland, V. Vaithyanathan, D. G. Schlom, U. V. Waghmare, N. A. Spaldin, K. M. Rabe, M. Wuttig and R. Ramesh, *Science*, 2003, **299**, 1719.
 - S. Li, J. Zhang, M. G. Kibria, Z. Mi, M. Chaker, D. Ma, R. Nechache and F. Rosei, *Chem. Commun.*, 2013, **49**, 5856.
 - X. Y. Chen, T. Yu, F. Gao, H. T. Zhang, L. F. Liu, Y. M. Wang, Z. S. Li and Z. G. Zou, *Appl. Phys. Lett.*, 2007, **91**, 022114; S. M. Sun, W. Z. Wang, L. Zhang and M. Shang, *J. Phys. Chem. C*, 2009, **113**, 12826.
 - T. Soltani and M. H. Entezari, *J. Mol. Catal. A: Chem.*, 2013, **377**, 197; Y. Liu, R. Zuo and S. Qi, *J. Mol. Catal. A: Chem.*, 2013, **376**, 1; Z. Li, Y. Shen, C. Yang, Y. Lei, Y. Guan, Y. Lin, D. Liu and C.-W. Nan, *J. Mater. Chem. A*, 2013, **1**, 823; Z. Li, Y. Shen, Y. Guan, Y. Hu, Y. Lin and C.-W. Nan, *J. Mater. Chem. A*, 2014, **2**, 1967.
 - F. Gao, X. Chen, K. Yin, S. Dong, Z. Ren, F. Yuan, T. Yu, Z. Zou and J.-M. Liu, *Adv. Mater.*, 2007, **19**, 2889.
 - L. Li, P. A. Salvador and G. S. Rohrer, *Nanoscale*, 2014, **6**, 24; Y. Zhang, A. M. Schultz, P. A. Salvador and G. S. Rohrer, *J. Mater. Chem.*, 2011, **21**, 4168.
 - W. Eerenstein, F. D. Morrison, J. Dho, M. G. Blamire, J. F. Scott and N. D. Mathur, *Science*, 2005, **307**, 1203.
 - T. Park, G. C. Papaefthymiou, A. J. Viescas, A. R. Moodenbough and S. S. Wong, *Nano Lett.*, 2007, **7**, 766.
 - X. Chen and S. S. Mao, *Chem. Rev.*, 2007, **107**, 2891.
 - X. Wang, Y. Lin, X. Ding and J. Jiang, *J. Alloys Comp.*, 2011, **509**, 6585; F. Gao, X. Chen, K. Yin, S. Dong, Z. Ren, F. Yuan, T. Yu, Z. Zou and J.-M. Liu, *Adv. Mater.*, 2007, **19**, 2889; Z. Bi, O. Anderoglu, X. Zhang, J. L. MacManus-Driscoll, H. Yang, Q. Jia and H. Wang, *Nanotechnology*, 2010, **21**, 285607.
 - Y. Huo, M. Miao, Y. Zhang, J. Zhu and H. Li, *Chem. Commun.*, 2011, **47**, 2089.
 - L. Xu, F.-X. Bu, M. Hu, C.-Y. Jin, D.-M. Jiang, Z.-J. Zhao, Q.-H. Zhang and J.-S. Jiang, *Chem. Commun.*, 2014, **50**, 13849.
 - M. K. Bhunia, S. K. Das, A. Dutta, A. Sengupta and A. Bhaumik, *J. Nanosci. Nanotechnol.*, 2013, **13**, 2557.
 - C. Reitz, C. Suchomski, C. Weidmann and T. Brezesinski, *Nano Res.*, 2011, **4**, 414.
 - I. Papadas, J. A. Christodoulides, G. Kioseoglou, G. S. Armatas, *J. Mater. Chem. A*, 2015, **3**, 1587.

Journal Name

- 17 S. Ghosh, S. Dasgupta, A. Sen and H. S. Maiti, *J. Am. Ceram. Soc.*, 2005, **88**, 1349.
- 18 M. T. S. Rosado, M. L. R. S. Duarte and R. Fausto, *J. Mol. Struct.*, 1997, **410-411**, 343.
- 19 A. V. Semenyuk and D. I. Svergun, *J. Appl. Crystallogr.*, 1991, **24**, 537.
- 20 F. Rouquerol, J. Rouquerol and K. S. W. Sing, *Adsorption by Powders and Porous Solids. Principles Methodology and Applications*, Academic Press, New York, 1999.
- 21 S. Brunauer, L. S. Deming, W. E. Deming and E. Teller, *J. Am. Chem. Soc.*, 1940, **62**, 1723.
- 22 P. I. Ravikovitch, D. Wei, W. T. Chueh, G. L. Haller and A. V. Neimark, *J. Phys. Chem. B*, 1997, **101**, 3671.
- 23 J. Tauc, *Mater. Res. Bullet.*, 1968, **3**, 37.
- 24 S. Li, Y.-H. Lin, B.-P. Zhang, Y. Wang and C.-W. Nan, *J. Phys. Chem. C*, 2010, **114**, 2903.
- 25 M. J. Vaidya, S. M. Kulkarni and R. V. Chaudhari, *Org. Process Res. Dev.*, 2003, **7**, 202.
- 26 N. Pradhan, A. Pal and T. Pal, *Langmuir*, 2001, **17**, 1800.
- 27 F.-h. Lin and R.-A. Doong, *J. Phys. Chem. C.*, 2011, **115**, 6591.
- 28 S. Y. Gao, X. X. Jia, Z. D. Li and Y. L. Chen, *J. Nanopart. Res.*, 2012, **14**, 1.
- 29 X. Q. Huang, Y. J. Li, H. L. Zhou, X. Zhong, X. F. Duan and Y. Huang, *Chem.-Eur. J.*, 2012, **18**, 9505.
- 30 Y. P. Xue, X. F. Lu, X. J. Bian, J. Y. Lei and C. Wang, *J. Colloid Interface Sci.*, 2012, **379**, 89.
- 31 J. F. Huang, S. Vongehr, S. C. Tang, H. M. Lu, J. C. Shen and X. K. Meng, *Langmuir*, 2009, **25**, 11890.
- 32 J. Huang, S. Vongehr, S. Tang, H. Lu and X. Meng, *J. Phys. Chem. C*, 2010, **114**, 15005.
- 33 X. Y. Li, X. Wang, S. Y. Song, D. P. Liu and H. J. Zhang, *Chem.-Eur. J.*, 2012, **18**, 7601.
- 34 S. Ghosh, S. Dasgupta, A. Sen and H. S. Maiti, *J. Am. Ceram. Soc.*, 2005, **88**, 1349.
- 35 F. A. P. Hammersley, *ESRF98HA01T: FIT2D V9.129 Reference Manual V3.1*, ESRF Internal Report, France, 1998.